Electronic Supporting Information (ESI)

High Proton Conduction by Full Hydration in Highly Oxygen Deficient Perovskite

Kei Saito,[a,†] Kensei Umeda,[a,†] Kotaro Fujii,[a] Kazuhiro Mori,[b,c,d] Masatomo Yashima[a,*]

[a] *Department of Chemistry, School of Science, Tokyo Institute of Technology, 2-12-1-W4-17, O-okayama, Meguro-ku, Tokyo 152-8551, Japan*

[b] *Institute of Materials Structure Science / J-PARC Center, High Energy Accelerator Research Organization (KEK), 203-1 Shirakata, Tokai, Ibaraki 319-1106, Japan.*

[c] *Graduate Institute for Advanced Studies, The Graduate University for Advanced Studies (SOKENDAI), 203-1 Shirakata, Tokai, Ibaraki 319-1106, Japan.*

[d] *Graduate School of Science and Engineering, Ibaraki University, 203-1 Shirakata, Tokai, Ibaraki 319-1106, Japan.*

* Corresponding author: yashima@cms.titech.ac.jp
† *K.S. and K.U. contributed equally to this work.*

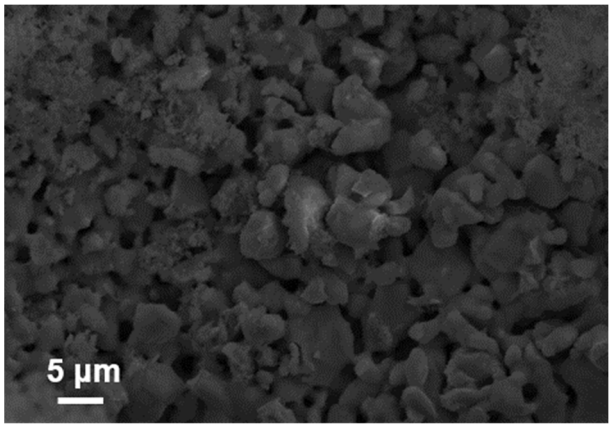

Figure S1. SEM micrograph of a sintered pellet of BSW. The sample was thermally etched at 1300 °C for 10 min prior to the SEM observation. The average grain size was estimated to be 3 μm in diameter.

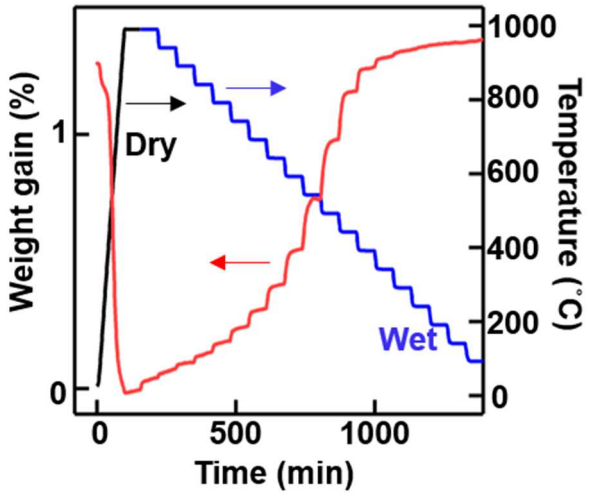

Figure S2. Water uptake of BSW in wet air.

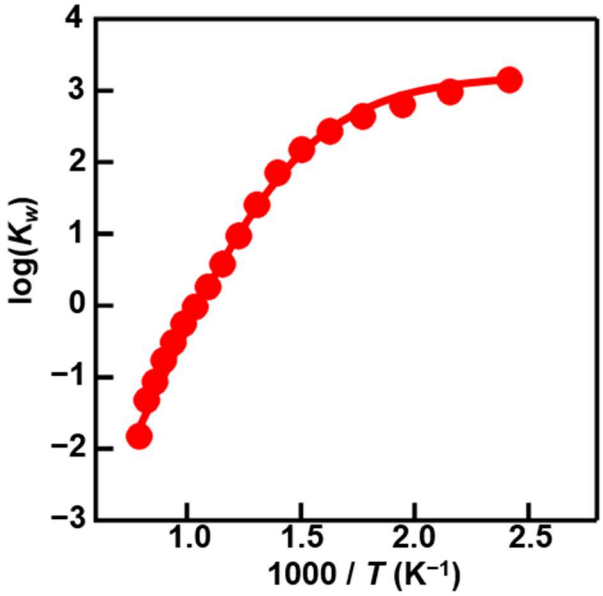

Figure S3. van 't Hoff plot of the equilibrium constant K_w for the hydration of BSW. The K_w was calculated using the equation in the literature.[1]

Table S1. Hydration enthalpy and entropy of $BaSc_{0.8}W_{0.2}O_{2.8-y/2}(OH)_y$ (BSW), $BaSc_{0.8}Mo_{0.2}O_{2.8-y/2}(OH)_y$ (BSM),[1] and $BaZr_{0.4}Sc_{0.6}O_{2.7-y/2}(OH)_y$ (BZS)[2] at 500−1000, 500−1000, and 450−1000 °C, respectively. The hydration enthalpy and entropy of BSW were estimated using the van 't Hoff plots (**Figure S3**).

Composition	$\Delta H°$ (kJ mol^{-1})	$\Delta S°$ (J K^{-1} mol^{-1})
$BaSc_{0.8}W_{0.2}O_{2.8-y/2}(OH)_y$	−111(5)	−117(5)
$BaSc_{0.8}Mo_{0.2}O_{2.8-y/2}(OH)_y$	−115(4)	−130(4)
$BaZr_{0.4}Sc_{0.6}O_{2.7-y/2}(OH)_y$	−121(2)	−117(2)

The hydration enthalpy and entropy of BSW have similar values with those of proton conducting perovskites BSM and BZS.

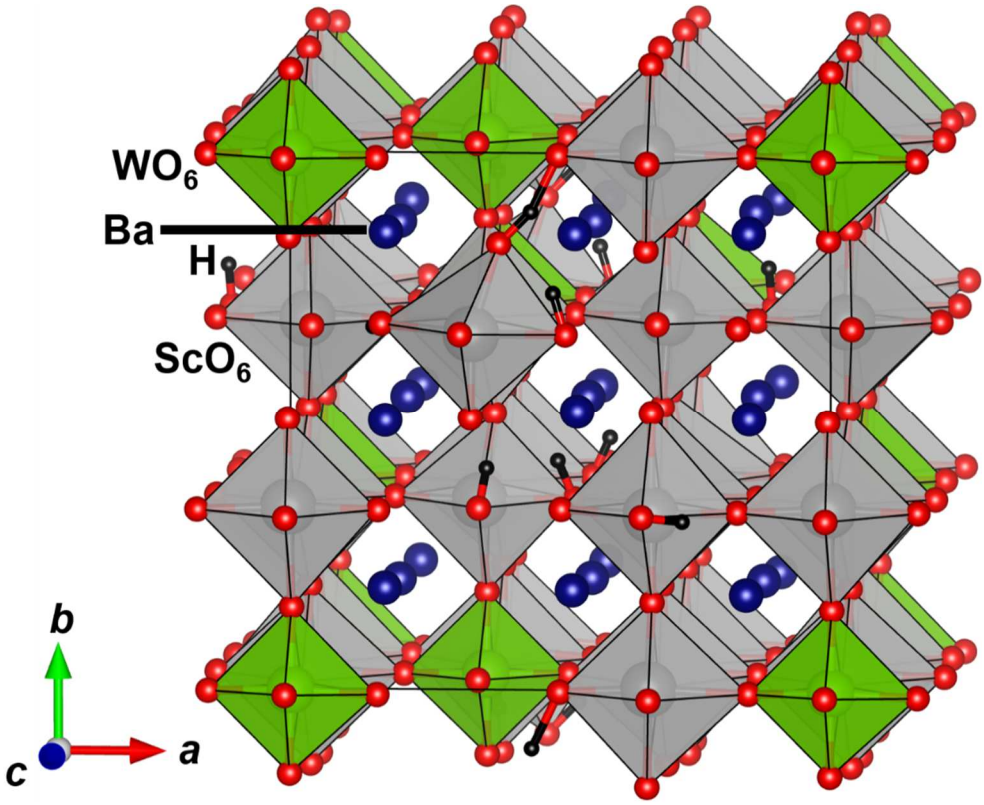

Figure S4. Optimized structure of $Ba_{27}Sc_{22}W_5O_{81}H_{12}$, which was obtained by static DFT calculations.

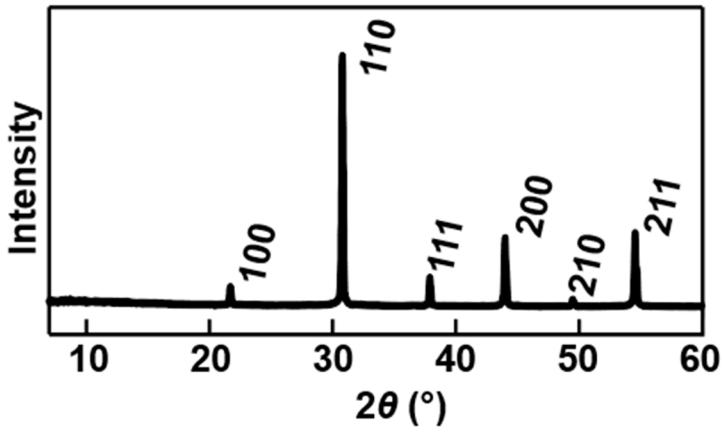

Figure S5. Cu Kα X-ray powder diffraction pattern of as-prepared BSW powders at 24 ºC. *hkl* denotes the reflection index of the primitive cubic cell.

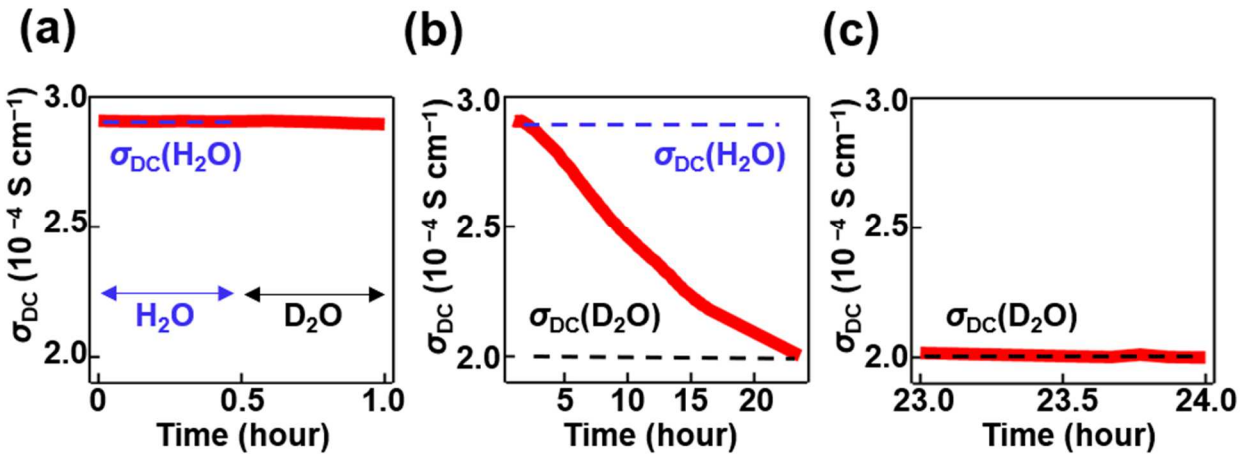

Figure S6. H/D isotope effect on the DC electrical conductivity of BSW at 250 °C during (a) 0−1 h, (b) 1−23 h, and (c) 23−24 h. $\sigma_{DC}(H_2O)$ and $\sigma_{DC}(D_2O)$ stand for the DC electrical conductivities in H_2O- and D_2O-saturated air, respectively.

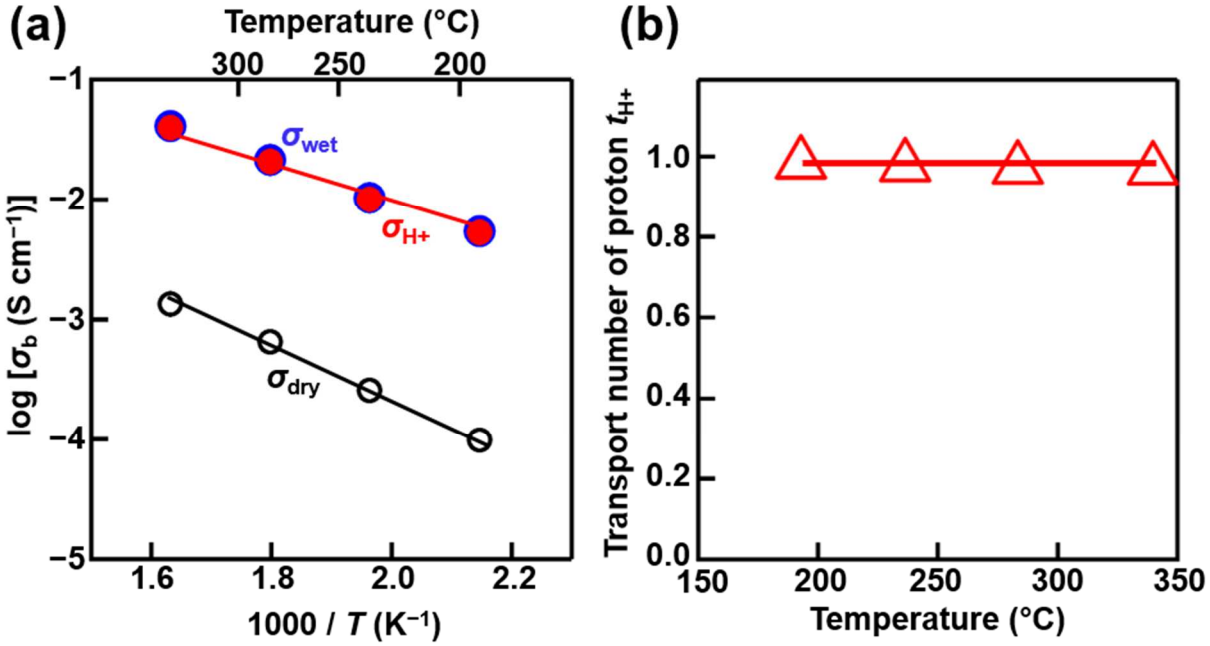

Figure S7. (a) Arrhenius plots of bulk conductivity of BSW in wet air (σ_{wet}, blue open circles) and dry air (σ_{dry}, black open circles and line). Arrhenius plots of the bulk proton conductivity of BSW (red closed circles and line). Here, the bulk proton conductivity σ_{H+} was estimated using the equation, $\sigma_{H+} = \sigma_{wet} - \sigma_{dry}$. (b) Temperature dependence of proton transport number in BSW. The proton transport number was calculated by the equation, $t_{H+} = \sigma_{H+}/\sigma_{wet}$.

ESI Note 1: Kramers-Kronig (KK) validation

Figure S8a shows the KK residuals of experimental data of BSW in wet air. The absolute values of the KK residual were lower than 0.7%. Figure S8b shows the equivalent circuit (EC) residual plots of BSW in wet air. The absolute values of the EC residual were lower than 0.1%. These residual values validate the collected impedance data.[3]

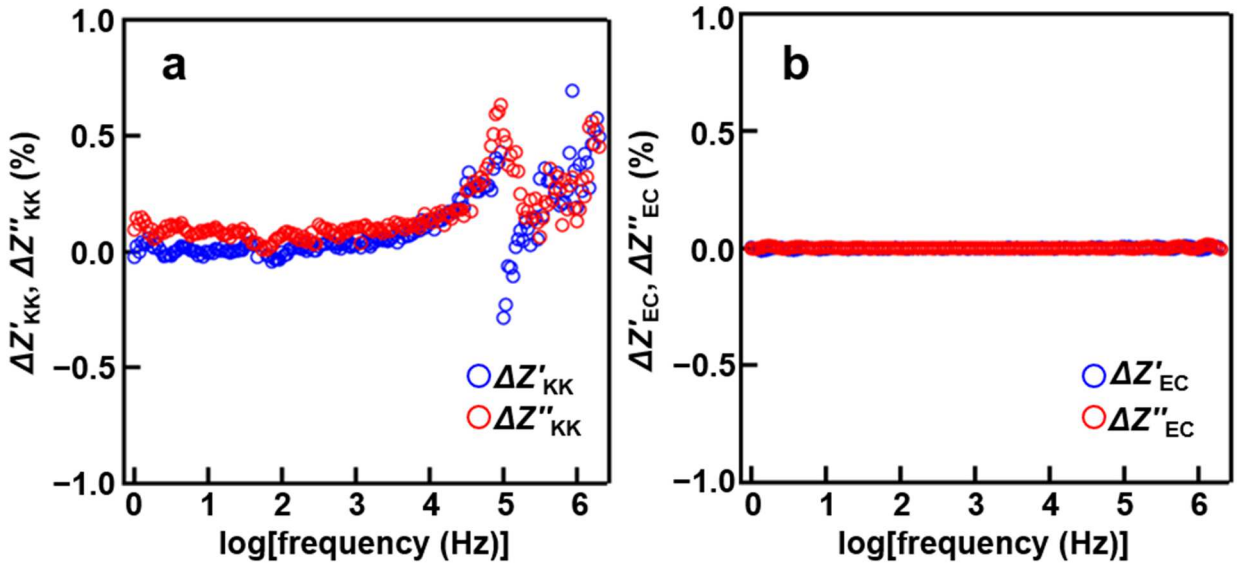

Figure S8. Residual plots of (a) the measured impedance data obtained by the Kramers-Kronig transformation and (b) the equivalent circuit fitting of BSW in wet air at 236 ºC.

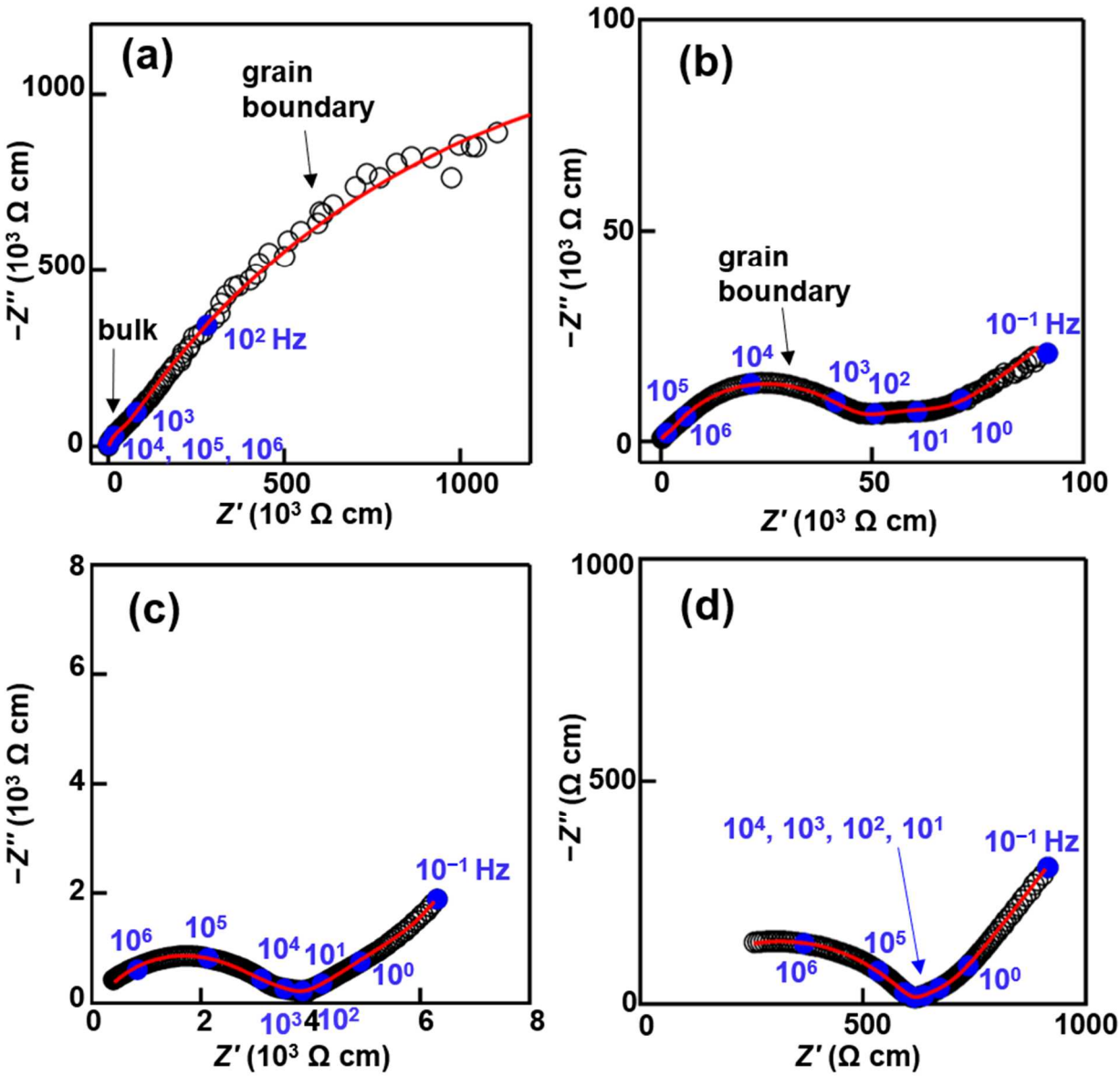

Figure S9. Complex impedance plots of BSW at (a) 46, (b) 143, (c) 236 and (d) 340 °C in wet air. Each number denotes the frequency at a blue closed circle. The red solid line represents the fitting curve.

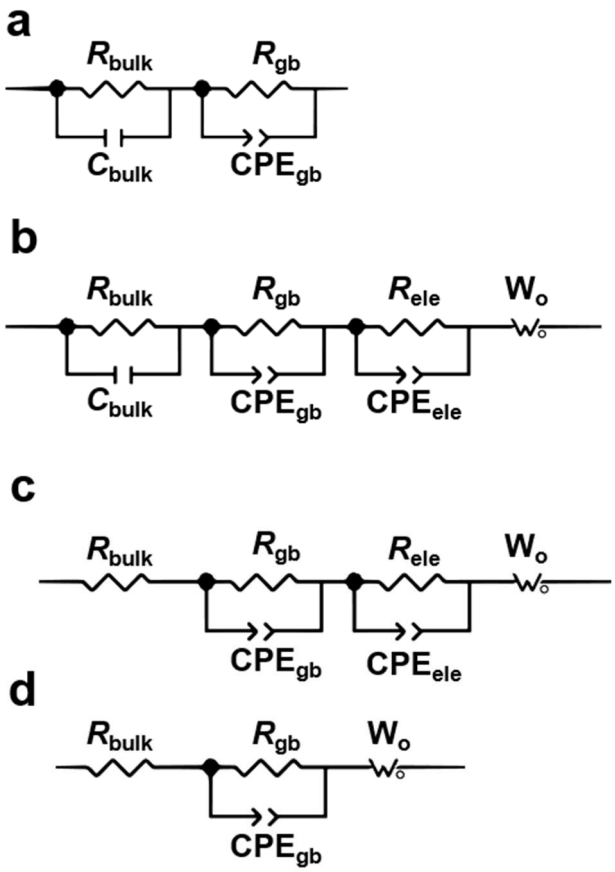

Figure S10. Equivalent circuits used to model the impedance spectra of BSW at (a) 46–90 °C, (b) 143 °C, (c) 193–236 °C, and (d) 283–446 °C. *R*, *C*, CPE, and W_o denote a resistance, capacitance, constant phase element, and open Warburg element, respectively. The subscripts "bulk", "gb", and "ele" denote the bulk, grain boundary, and electrode, respectively.

Table. S2. Capacitances for bulk C_b and grain boundary C_{gb} of BSW in wet air.

T (°C)	C_b (F)	C_{gb} (F)
46	$2.8(2)\times10^{-11}$	$1.62(3)\times10^{-10}$
90	$1.85(9)\times10^{-11}$	$2.3163(8)\times10^{-10}$
143	$1.85(6)\times10^{-11}$	$7.28(6)\times10^{-11}$
193		$5.749(7)\times10^{-11}$
236		$3.67(6)\times10^{-11}$
283		$3.187(4)\times10^{-11}$
340		$2.539(1)\times10^{-11}$
393		$2.086(1)\times10^{-11}$
446		$1.694(5)\times10^{-11}$

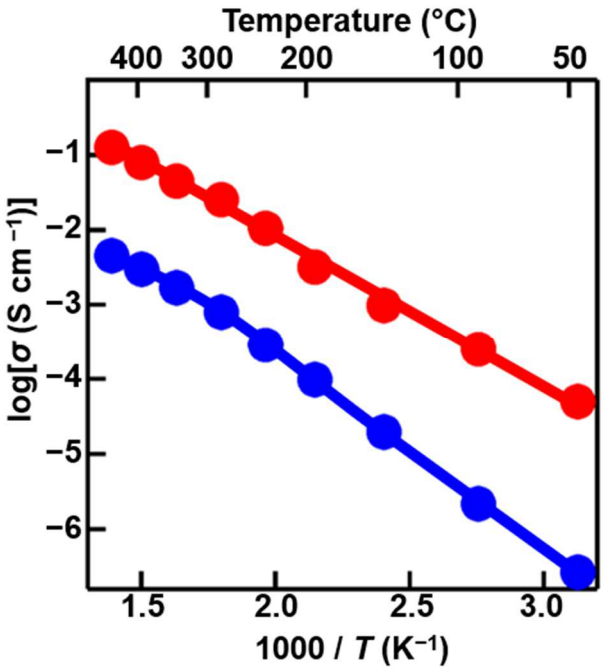

Figure S11. Arrhenius plots of bulk (red circles) and grain-boundary (blue circles) conductivities of BSW in wet air. The activation energy for bulk conductivity was calculated to be 0.40 eV. The activation energies for grain boundary conductivity were calculated to be 0.53 eV from 46 to 283 °C and 0.36 eV from 283 to 446 °C.

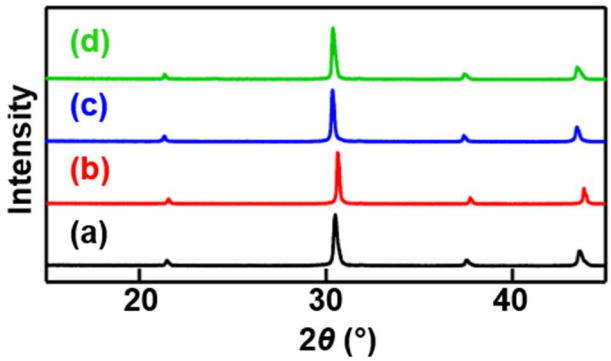

Figure S12. Cu Kα X-ray powder diffraction patterns of BSW (a) before annealing, after annealing at 450 °C under (b) CO_2 for 200 h and (c) H_2 for 100 h, and (d) after standing under ambient atmosphere (in ambient air with 50–80% relative humidity and CO_2) at room temperature for 100 h.

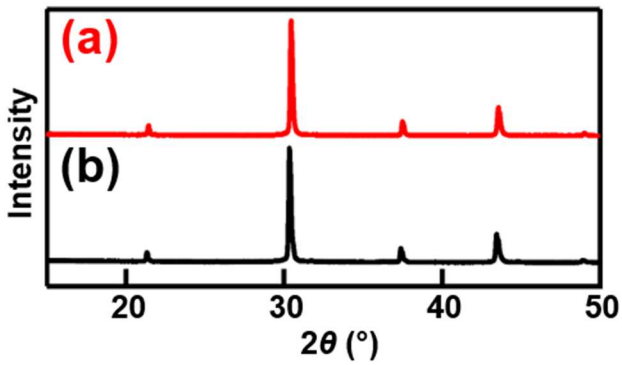

Figure S13. Cu Kα X-ray powder diffraction patterns of (a) the BSW sample after the electrical conductivity measurements through three heating and cooling cycles and (b) as-prepared BSW sample.

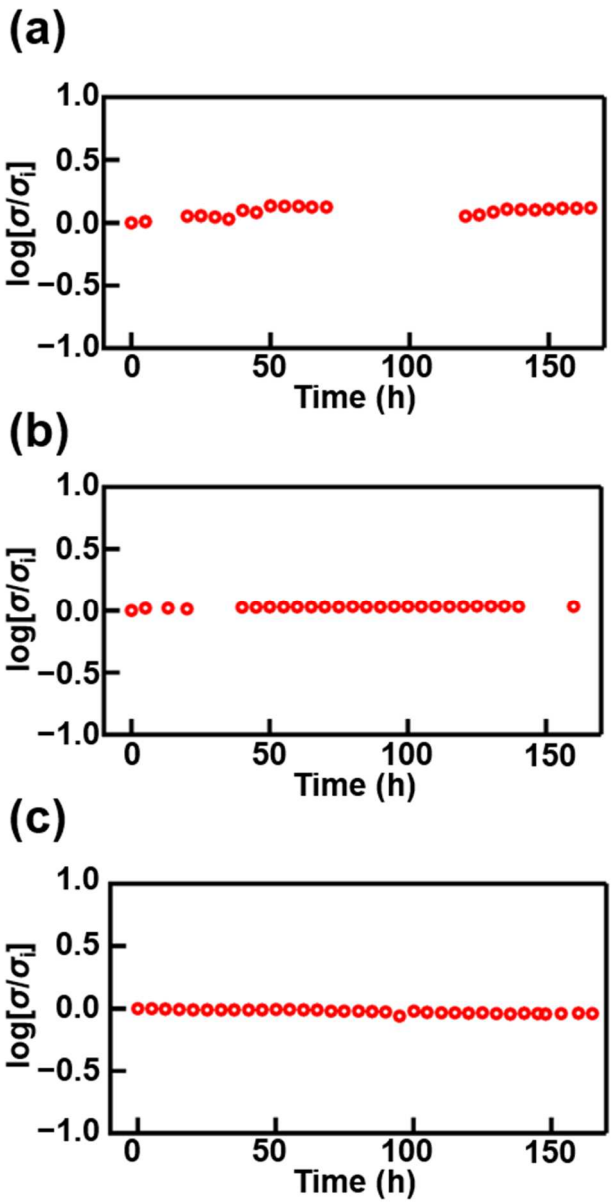

Figure S14. Stability of the electrical conductivity σ under (a) wet H_2, (b) wet air, and (c) wet CO_2 atmospheres at 450 °C. σ_i denotes the initial electrical conductivity (σ at 0 h).

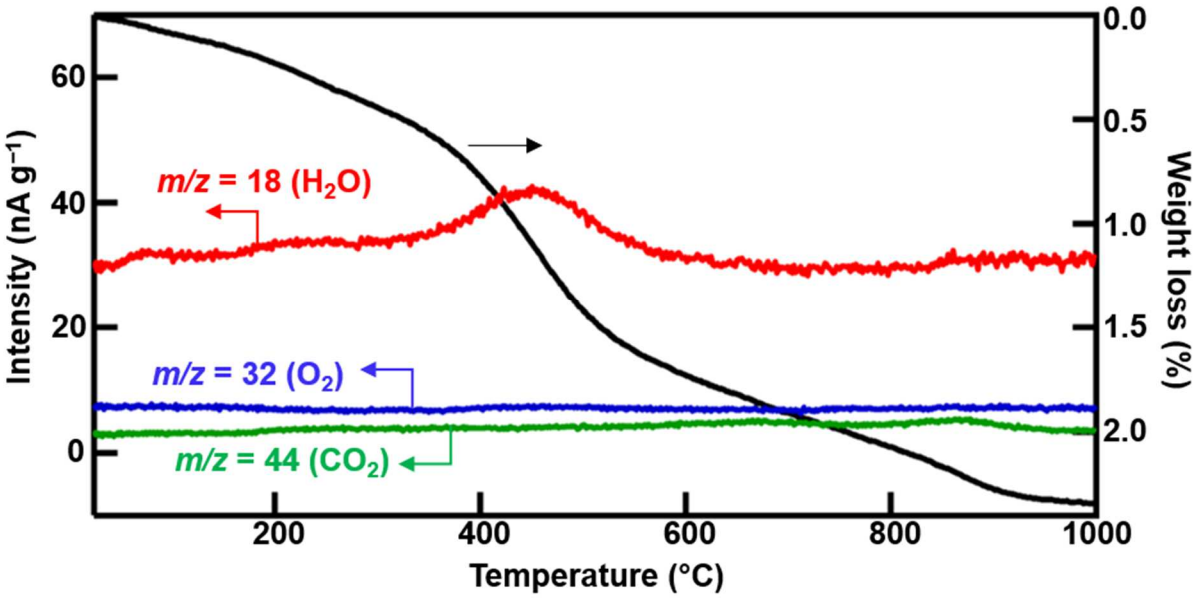

Figure S15. Thermogravimetric-mass spectrometric (TG-MS) data of wet BSW powders measured under dry He flow. The sample weight decreased during heating. TG-MS data showed that the weight loss was mainly due to the dehydration (water evaporation, *m/z* = 18, red line). Additional weight loss at high temperatures was caused by the release of CO_2 gas (*m/z* = 44, green line). O_2 from the sample was not detected (*m/z* = 32, blue line).

Table S3. Atomic coordinates of hydrogen atom of BSW and $BaSc_{0.8}Mo_{0.2}O_{2.8-y/2}(OD)_y$ (Ref. [1]), which were refined by Rietveld analysis of neutron diffraction data. Average atomic coordinates of proton of $Ba_{27}Sc_{22}W_5O_{69}(OH)_{12}$, which were optimized by DFT calculations. The refined atomic coordinates *x* and *y* of D atom in BSW were in agreement with those of $BaSc_{0.8}Mo_{0.2}O_{2.8-y/2}(OD)_y$ (Ref. [1]) within four and three estimated standard deviations, respectively. The refined atomic coordinates *x* and *y* of D atom in BSW were in agreement with the average atomic coordinates optimized by the DFT calculations within 2% and 2.8%, respectively.

Composition	Atomic coordinates of hydrogen atom		
	x	*y*	*z*
$BaSc_{0.8}W_{0.2}O_{2.600(12)}(OD)_{0.40(2)}$	0.449(6)	0.248(6)	0
$Ba_{27}Sc_{22}W_5O_{69}(OH)_{12}$	0.43	0.22	0.00
$BaSc_{0.8}Mo_{0.2}O_{2.6400(15)}(OD)_{0.3173(17)}$	0.4254(10)	0.2307(15)	0

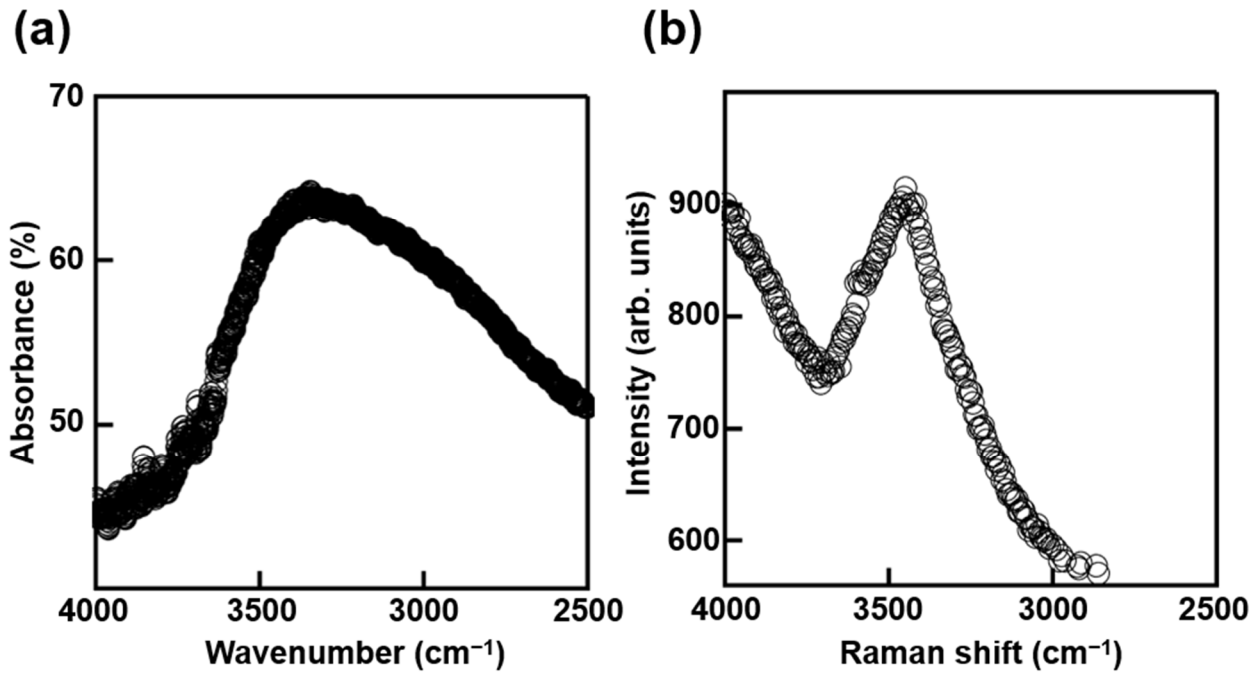

Figure S16. (a) IR and (b) Raman spectra of wet BSW powders. Novak proposed an empirical equation to express the correlation between OH bond length and frequency using data of 21 materials.[4] Using the empirical equation, the OH bond length of the wet BSW powders was estimated to be 1.00 Å from IR data and 0.99 Å from Raman data.

Table S4. Fractional water uptake F_w of $BaSc_{0.8}W_{0.2}O_{2.8-y/2}(OH)_y$ (BSW), $BaSc_{0.8}Mo_{0.2}O_{2.8-y/2}(OH)_y$ (BSM),[1] $BaSc_{0.75}Mo_{0.25}O_{2.875-y/2}(OH)_y$ (Ref. [1]), $BaZr_{0.8}Y_{0.2}O_{2.9-y/2}(OH)_y$ (Ref. [5]), and $BaCe_{0.9}Y_{0.1}O_{2.95-y/2}(OH)_y$ (Ref. [6]).

Composition	F_w
$BaSc_{0.8}W_{0.2}O_{2.8-y/2}(OH)_y$	1.00
$BaSc_{0.8}Mo_{0.2}O_{2.8-y/2}(OH)_y$	0.80
$BaSc_{0.75}Mo_{0.25}O_{2.875-y/2}(OH)_y$	0.48
$BaZr_{0.8}Y_{0.2}O_{2.9-y/2}(OH)_y$	0.87
$BaCe_{0.9}Y_{0.1}O_{2.95-y/2}(OH)_y$	0.84

ESI Note 2: Higher fractional water uptake F_w in BSW compared with BSM due to the larger lattice volume

The fractional water uptake F_w of $BaSc_{1-x}M_xO_{3-\delta}$ increases with increasing the experimental lattice volume V (Figure S17a), which is supported by the increase of F_w with an increase of the "average lattice volume" $\langle V_c \rangle$ (Figure S17b) where the $\langle V_c \rangle$ is defined below*. Therefore, the higher F_w of BSW compared with BSM can be attributed to the larger lattice volume V of BSW compared with BSM. The $\langle V_c \rangle$ of $BaSc_{0.8}M_{0.2}O_{3-\delta}$ can be expressed as

$\langle V_c \rangle = (0.2r_M + 4.124)^3$ [Å^3]. Here, r_M is the ionic radius of donor dopant M^{6+} cation for the coordination number (CN) of 6 (M = W for BSW and M = Mo for BSM). The $\langle V_c \rangle$ of $BaSc_{0.8}M_{0.2}O_{3-\delta}$ increases with an increase of r_M. Since the r_W is larger than r_{Mo}, $\langle V_c \rangle$ of BSW is larger than that of BSM. Thus, the higher F_w of BSW compared with BSM is attributable to the larger ionic radius of W^{6+} cation compared with Mo^{6+}.

*The "average lattice volume" $\langle V_c \rangle$ is defined by the equation,

$\langle V_c \rangle = ((2(r_{Sc/M} + r_O) + \sqrt{2}(r_{Ba} + r_O))/2)^3$, where r_{Ba} and r_O are the ionic radii of Ba^{2+} for the CN of 12 and O anion (O^{2-}) for the CN of 6, respectively. The $r_{Sc/M}$ was calculated by the equation, $r_{Sc/M} = (1-x)r_{Sc} + xr_M$ where r_{Sc} and r_M are the ionic radii of Sc and M cations, respectively, for CN = 6 in $BaSc_{1-x}M_xO_{3-\delta}$.

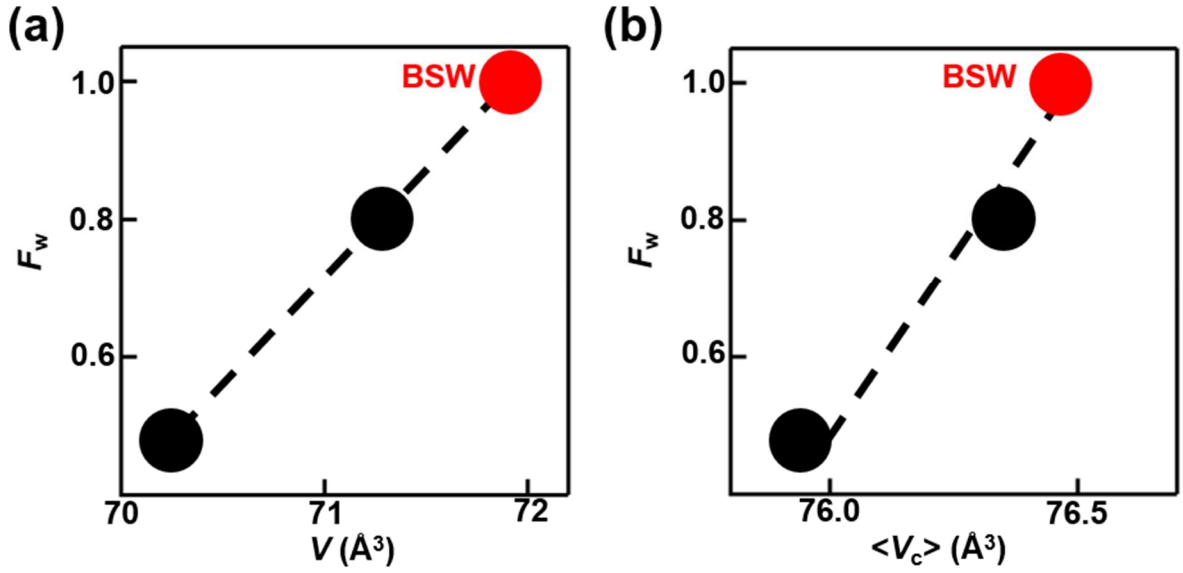

Figure S17. Variation of the fractional water uptake F_w with (a) experimental lattice volume V and (b) average lattice volume $\langle V_c \rangle$. Red circle denotes BSW. Black circles represent BSM and $BaSc_{0.75}Mo_{0.25}O_{2.875-y/2}(OH)_y$.[1]

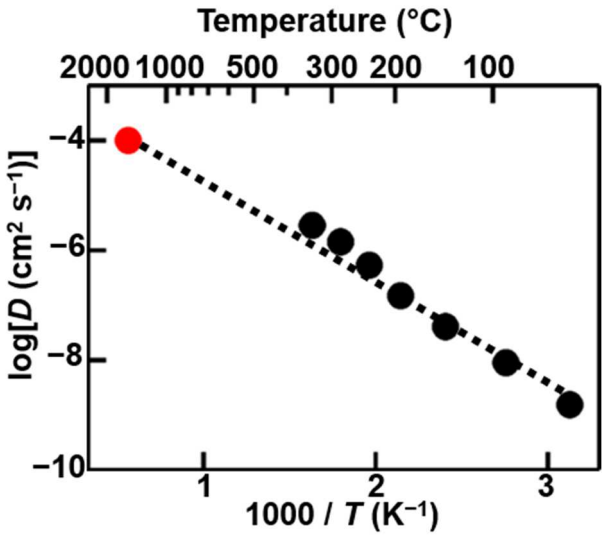

Figure S18. Comparison of the experimental *D* of BSW (black circles) with the *D* calculated by AIMD simulations (red circle). Dotted line is the guide for eyes.

References

1 K. Saito, M. Yashima, *Nat. Commun.*, 2023, **14**, 7466.

2 J. Hyodo, K. Kitabayashi, K. Hoshino, Y. Okuyama, Y. Yamazaki, *Adv. Energy Mater.*, 2020, **10**, 2000213.

3 B. A. Boukamp, *J. Electrochem. Soc.*, 1995, **142**, 1885.

4 A. Novak, Hydrogen bonding in solids correlation of spectroscopic and crystallographic data. in *Large Molecules*, Springer, Berlin, Heidelberg, 1974; 177–216.

5 J. Hyodo, K. Tsujikawa, M. Shiga, Y. Okuyama, Y. Yamazaki, *ACS Energy Lett.*, 2021, **6**, 2985.

6 K. D. Kreuer, *Annu. Rev. Mater. Res.*, 2003, **33**, 333.